

Frequency Domain Nuances Mining for Visible-Infrared Person Re-identification

Yukang Zhang^{1,2}, Yang Lu^{1,2}, Yan Yan^{1,2}, Hanzi Wang^{1,2*}, Xuelong Li³

¹Fujian Key Laboratory of Sensing and Computing for Smart City,
School of Informatics, Xiamen University, 361005, P.R. China.

²Key Laboratory of Multimedia Trusted Perception and Efficient Computing,
Ministry of Education of China, Xiamen University, 361005, P.R. China.

³Northwestern Polytechnical University, Xi'an, Shaanxi, China.

zhangyk@stu.xmu.edu.cn, {luyang, yanyan, hanzi.wang}@xmu.edu.cn, li@nwpu.edu.cn

Abstract

The key of visible-infrared person re-identification (VIREID) lies in how to minimize the modality discrepancy between visible and infrared images. Existing methods mainly exploit the spatial information while ignoring the discriminative frequency information. To address this issue, this paper aims to reduce the modality discrepancy from the frequency domain perspective. Specifically, we propose a novel Frequency Domain Nuances Mining (FDNM) method to explore the cross-modality frequency domain information, which mainly includes an amplitude guided phase (AGP) module and an amplitude nuances mining (ANM) module. These two modules are mutually beneficial to jointly explore frequency domain visible-infrared nuances, thereby effectively reducing the modality discrepancy in the frequency domain. Besides, we propose a center-guided nuances mining loss to encourage the ANM module to preserve discriminative identity information while discovering diverse cross-modality nuances. Extensive experiments show that the proposed FDNM has significant advantages in improving the performance of VIREID. Specifically, our method outperforms the second-best method by 5.2% in Rank-1 accuracy and 5.8% in mAP on the SYSU-MM01 dataset under the indoor search mode, respectively. Besides, we also validate the effectiveness and generalization of our method on the challenging visible-infrared face recognition task. *The code will be available.*

1. Introduction

Visible-infrared (VIS-IR) person re-identification (VIREID) is attracting increasing attention due to its enormous potential in surveillance systems [31]. Given a query image, the goal of VIREID is to match the VIS person images

*Corresponding author.

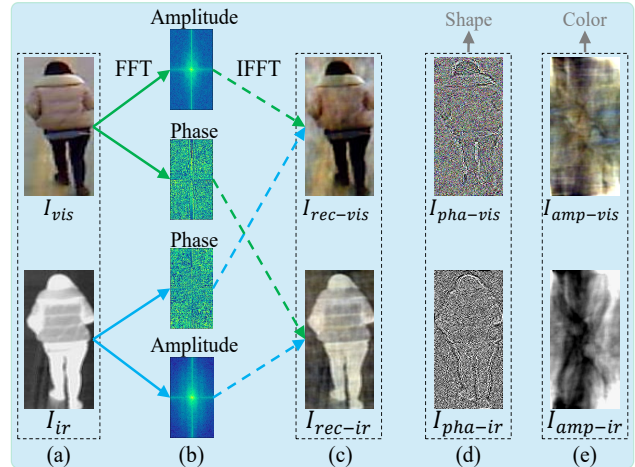


Figure 1. Decomposition and reconstruction of the VIS and IR images in the frequency domain. (a) denote the VIS and IR images; (b) are the amplitude and phase components of the VIS and IR images in the frequency domain; (c) are the reconstructed images of swapping the amplitude and phase components of the VIS and IR images; (d) are the reconstructed VIS and IR images with phase component information only; (e) are the reconstructed VIS and IR images with amplitude component information only.

with corresponding IR person images in a non-overlapping camera surveillance system. The VIREID is challenging due to the large modality discrepancy between the VIS and IR images, resulting in significant intra-modality and inter-modality variations [24, 49, 50]. Existing methods primarily focus on designing complex networks or loss functions to extract modality-invariant discriminative features [2, 3, 11]. Although these methods have made remarkable progress in VIREID, they mainly exploit the spatial information but neglect the discriminative frequency information.

Recently, frequency domain feature learning has demonstrated its strong advantages in different tasks, such as image defogging [55], image exposure correction [16], and domain generalization [19]. Compared to the spatial domain

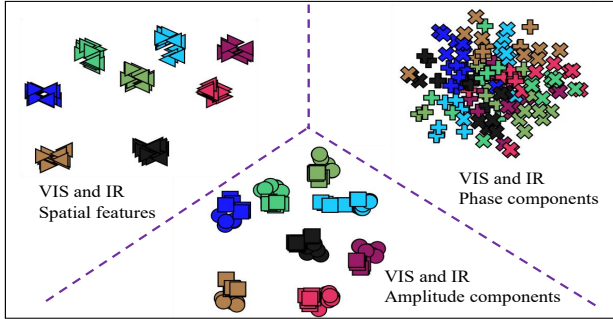


Figure 2. The t-SNE [18] for the VIS and IR features of spatial domain and frequency domain. The samples with the same color are from the same persons. It is apparent that the spatial features and the features of the amplitude component are discriminative while the features of the phase component contain key missing information for the VIREID task.

information, the difference between the VIS and IR images in the frequency domain is physically defined. As shown in Fig. 1, when reconstructing images by swapping the amplitude and phase components of the VIS and IR images, the resulting images have the same amplitude components but different phase components, making them visually similar. Besides, the images reconstructed by the phase components and the amplitude components preserve the shape and color information of person images, respectively. These results show that the amplitude components obtained by the Fourier transform contain key information for the VIREID task. Additionally, we also visualize the distribution of different features using t-SNE [18] in Fig. 2. It is apparent that the distribution of the spatial features and amplitude components are distinguished, while the phase components contain important missing information. Thus, alleviating the modality discrepancy between the VIS and IR images and mining the cross-modality nuances in the frequency domain are of great importance for the VIREID task.

Based on the above observation, we propose an effective frequency domain nuances mining (FDNM) method for the VIREID task. The proposed FDNM aims to enable the phase component to learn discriminative information and mine the diverse cross-modality nuances contained in the amplitude component. Therefore, we propose two key modules: an amplitude guided phase (AGP) module and an amplitude nuances mining (ANM) module. The proposed AGP module extracts the key information of the amplitude component to guide the learning of the phase component, and improve the discriminative ability of the phase component for cross-modality information. It enables the proposed method to effectively reduce the modality discrepancy between VIS and IR images in the frequency domain. The proposed ANM module is to fully explore the influence of cross-modality nuances in the amplitude component. To encourage the proposed ANM module to discover robust VIS-IR nuances, we propose an effective center-guided nu-

ances mining loss, which can significantly improve the discriminative power of the proposed method. By combining the above two modules into an end-to-end network, the proposed FDNM can fully explore and utilize the diverse information in the frequency domain, significantly reducing the modality discrepancy between VIS and IR images. Extensive experiments show that the proposed FDNM achieves an impressive performance on three challenging VIREID datasets. The main contributions of this paper can be summarized as follows:

- We propose a novel frequency domain nuances mining method to exploits the potential frequency information for the VIREID task.
- We propose an amplitude guided phase module to exploit the key information of the amplitude component to promote the learning of the phase component, which improves the discriminative ability of the phase component and enables the proposed method to effectively learn robust VIS-IR feature representations.
- We propose an amplitude nuances mining module with a center-guided nuances mining loss to fully exploit the diverse cross-modality nuances contained in the amplitude component, which can significantly improve the performance of the proposed method.
- Extensive experiments show that the proposed method outperforms several state-of-the-art methods by a remarkable margin on three challenging VIREID datasets. Besides, we also validate the effectiveness and generalization of our method on the challenging VIS-IR face recognition task.

2. Related Work

2.1. Visible-Infrared Person Re-identification

To reduce the VIS-IR modality discrepancy, numerous works have been proposed and achieved impressive performance [42, 51]. Specifically, some image-level methods [4, 36–38] seek to generate pairs of the VIS-IR images for alleviating the modality gaps and improving the performance of the VIREID model. However, the lack of paired VIS-IR images may affect the quality and stability of the generated images. To address this issue, some lightweight networks [20, 40, 60] apply a channel-level grayscale transformation to introduce another modality for assisting the VIS-IR match task. However, those methods cannot obtain consistent person poses of the VIS and IR images [27].

The other methods [10, 30, 46] try to find a latent feature space, where the VIS-IR modality discrepancy can be reduced. For instance, PartMix [17] proposes to synthesize both positive and negative features and select reliable features to regularize the VIREID model. SGIEL [8] proposes to jointly optimize shape-related and shape-erased objectives to learn modality-shared features. DEEN [59] generates diverse embeddings and mines the channel-wise and

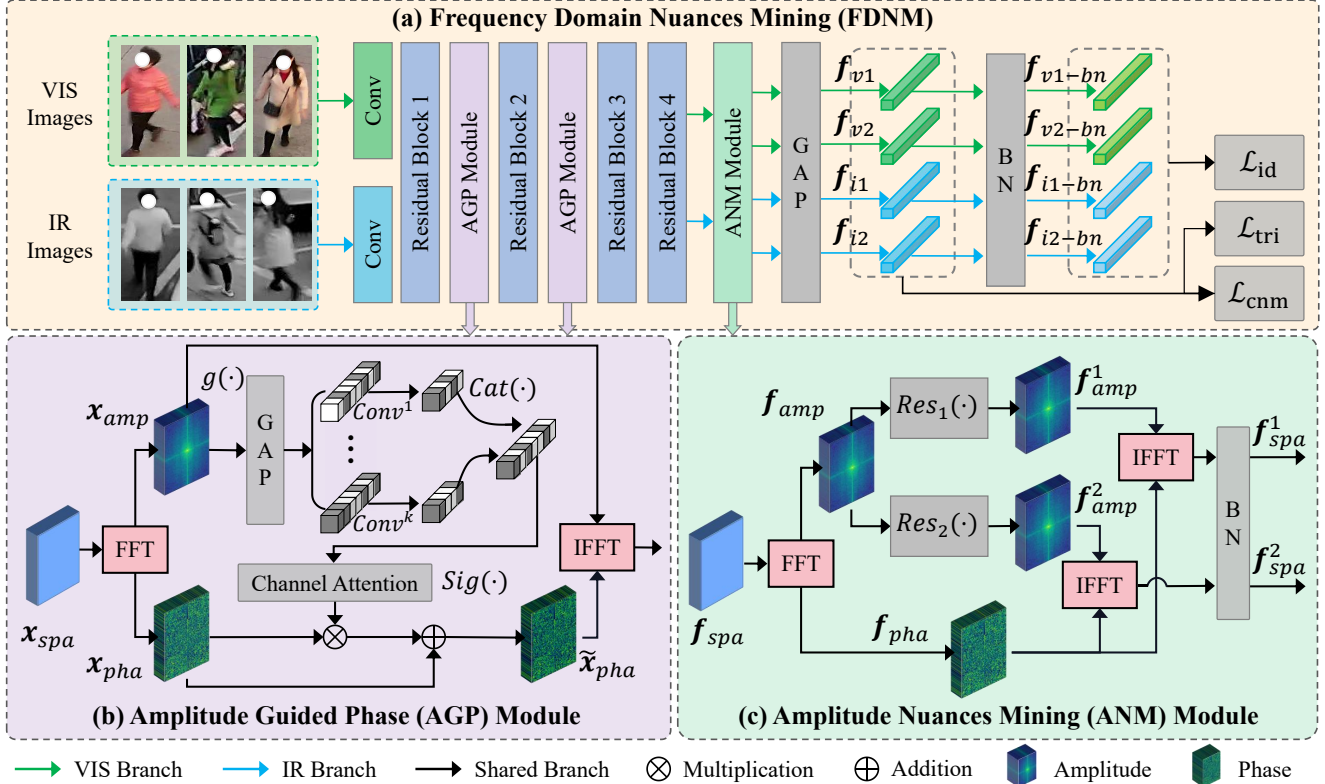


Figure 3. Overview of the proposed FDNM framework for the VIREID task. The proposed FDNM mainly includes an amplitude guided phase (AGP) module and an amplitude nuances mining (ANM) module to reduce the modality discrepancy between VIS and IR images in the frequency domain. After the GAP layer, we propose a center-guided nuances mining loss \mathcal{L}_{cnm} to encourage the proposed ANM module to preserve discriminative identity information while discovering diverse cross-modality nuances.

spatial embeddings to learn the informative features for reducing the VIS-IR modality discrepancy. SAAI [7] proposes to align latent semantic parts by considering the similarity between pixel-level features and learnable prototypes. Although these methods have made impressive progress, they mainly exploit the spatial information but neglect the discriminative frequency information.

2.2. Fourier Transform

The Fourier transform is widely used to analyze the frequency content, and numerous studies have demonstrated its effectiveness for addressing different tasks. For example, FECNet [16] introduces a Fourier-based exposure correction network to restore the amplitude and phase representations, thereby improving the lightness information for the exposure correction task. SFII [64] introduces a spatial-frequency information integration method to learn the effective information representation for the pan-sharpening task. FSDGN [55] proposes a frequency-spatial dual-guidance network to explore frequency-spatial domain potentials for the haze degradation task. SFMNet [35] designs a frequency-spatial interaction network to fuse frequency and spatial information and boost the face super-resolution

performance. CSNorm [48] designs an amplitude-based perturbation module to extract the essential information of lightness for the lightness adaptation task. FSI [22] proposes to eliminate the various diffractions and reconstruct the textures in the frequency and spatial domains. FDMNet [21] proposes a novel frequency domain modality-invariant feature learning framework to reduce modality discrepancy from the frequency domain perspective. Motivated by the success of these works, we propose a frequency domain nuances mining method for the VIREID task to exploit cross-modality nuances in the frequency domain.

3. Methodology

3.1. Basics of Fast Fourier Transform

The key of the VIREID task lies in minimizing the modality discrepancy between VIS and IR images. Previous works mainly exploit the spatial information while neglecting the discriminative frequency information, which is crucial for improving the performance of VIREID models. Therefore, before introducing the proposed FDNM, we first review the basics of the fast Fourier transform (FFT). Given a feature $\mathbf{x} \in \mathbb{R}^{C \times H \times W}$ output by network, the FFT of the feature \mathbf{x}

can be expressed as:

$$\mathcal{F}(\mathbf{x})(u, v) = \frac{1}{\sqrt{HW}} \sum_{h=0}^{H-1} \sum_{w=0}^{W-1} \mathbf{x}(h, w) e^{-2j\pi(\frac{h}{H}u + \frac{w}{W}v)}, \quad (1)$$

where j is the imaginary unit. u and v represent the horizontal and vertical coordinates of the feature \mathbf{x} . $\mathcal{F}(\mathbf{x})$ represents the FFT of feature \mathbf{x} . Accordingly, $\mathcal{F}^{-1}(\mathbf{x})$ represents the inverse fast Fourier transform (IFFT) of the feature \mathbf{x} . In the proposed FDNM, the FFT and IFFT are computed separately on each channel of feature maps.

In the frequency domain, $\mathcal{F}(\mathbf{x})(u, v)$ can be represented by the amplitude component \mathbf{x}_{amp} and the phase component \mathbf{x}_{pha} , which can be expressed as:

$$\mathbf{x}_{amp}(u, v) = \sqrt{R^2(\mathbf{x})(u, v) + I^2(\mathbf{x})(u, v)}, \quad (2)$$

$$\mathbf{x}_{pha}(u, v) = \arctan\left(\frac{I(\mathbf{x})(u, v)}{R(\mathbf{x})(u, v)}\right), \quad (3)$$

where $R(\mathbf{x})$ and $I(\mathbf{x})$ are the real and imaginary part of $\mathcal{F}(\mathbf{x})$, respectively.

In the frequency domain, the amplitude component \mathbf{x}_{amp} is mainly affected by brightness, contrast and modality discrepancy. The phase component \mathbf{x}_{pha} includes the structure information of the feature \mathbf{x} [55, 64]. Thanks to the FFT, the amplitude component \mathbf{x}_{amp} and phase component \mathbf{x}_{pha} can capture the global receptive field, which meets the demand of the VIREID task for effective long-distance dependency modeling and extracting modality-invariant feature representations. Additionally, it can be observed from Fig. 2 that the amplitude component \mathbf{x}_{amp} and the phase component \mathbf{x}_{pha} can capture different cross-modality features. Therefore, by modeling the amplitude component \mathbf{x}_{amp} and the phase component \mathbf{x}_{pha} , the modality discrepancy between VIS and IR images can be effectively reduced, and thus helping improve the performance of the VIREID model.

3.2. Overview

Based on the above analysis, we propose an effective frequency domain nuances mining (FDNM) method. As shown in Fig. 3, the proposed FDNM mainly includes an amplitude guided phase (AGP) module and an amplitude nuances mining (ANM) module to alleviate the modality discrepancy between VIS and IR images in the frequency domain. To improve the performance of the proposed FDNM, we combine the global and local feature representations for integrating discriminative information (for an intuitive display, only the global features are shown in Fig. 2. The local features have similar losses and displays. The parts are set to 4.). After the residual block 4 and global average pooling (GAP), a batch normalization (BN) layer is applied to stabilize the training process [26], which is parameter-shared among the two modalities.

3.3. Amplitude Guided Phase (AGP) Module

The proposed amplitude guided phase (AGP) module aims to utilize the key information in the amplitude component to guide the phase component for learning discriminative feature representations and reducing the modality discrepancy between the VIS and IR images.

To achieve this, as shown in Fig. 3 (b), the input features $\mathbf{x}_{spa} \in \mathbb{R}^{C \times H \times W}$ of the AGP module are first transformed into the frequency domain by FFT to obtain its amplitude components $\mathbf{x}_{amp} \in \mathbb{R}^{C \times H_1 \times W_1}$ and the phase components $\mathbf{x}_{pha} \in \mathbb{R}^{C \times H_1 \times W_1}$. Then, the amplitude components \mathbf{x}_{amp} are fed into a global average pooling layer $g(\cdot)$ and K 1×1 convolutional layers $Conv^K(\cdot) = \{Conv^k(\cdot)\}_{k=1}^K$ with non-shared parameters to reduce its dimension to C/K and extract robust amplitude components. Then, the K amplitude components are concatenated to restore its dimension back to C and fed into a sigmoid activation function $Sig(\cdot)$ to obtain the key amplitude information $\mathcal{S}(\mathbf{x}_{amp})$, which can be expressed as follows:

$$\mathcal{S}(\mathbf{x}_{amp}) = Sig(Cat(Conv^K(g(\mathbf{x}_{amp}))), \quad (4)$$

where $Cat(\cdot)$ denotes the concatenate operation.

As mentioned above, the amplitude components include key information for VIREID. Therefore, we utilize these key amplitude information $\mathcal{S}(\mathbf{x}_{amp})$ to guide the phase component for learning discriminative feature representations, as shown in Fig. 3 (b), which can be expressed as follows:

$$\tilde{\mathbf{x}}_{pha} = \mathcal{S}(\mathbf{x}_{amp}) \otimes \mathbf{x}_{pha} + \mathbf{x}_{pha}. \quad (5)$$

Finally, the amplitude components \mathbf{x}_{amp} and the obtained guided phase components $\tilde{\mathbf{x}}_{pha}$ are transformed back into the spatial domain features using the IFFT. By incorporating the proposed AGP module into the backbone network, we can effectively enhance the ability to extract discriminative features and alleviate the VIS-IR modality discrepancy in the frequency domain, ultimately leading to improved performance in the VIREID task.

3.4. Amplitude Nuances Mining (ANM) Module

As shown in Fig. 3 (c), the proposed amplitude nuances mining (ANM) module aims to discover the cross-modality nuances between the VIS and IR images in the frequency domain with a dual-branch structure. By mining diverse information contained in the amplitude component, the proposed ANM module can in turn promote the learning of the AGP module on the phase component, thereby effectively improving the performance of the VIREID task.

Specifically, the proposed ANM module first transforms the features \mathbf{f}_{spa} output by the last stage of the backbone into the frequency domain by FFT to obtain its amplitude components \mathbf{f}_{amp} and the phase components \mathbf{f}_{pha} . Then, two 1×1 convolutional blocks $Res_1(\cdot)$ and $Res_2(\cdot)$ are

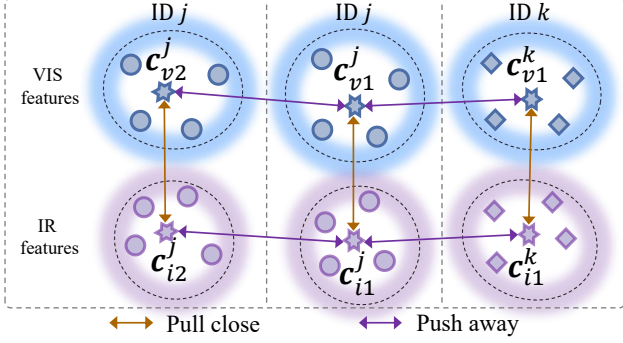


Figure 4. Illustration of the proposed center-guided nuances mining loss, which is used to preserve discriminative identity information while discovering diverse cross-modality nuances.

applied to learn diverse amplitude component nuances, with two Instance Normalization (IN) layers [34] to alleviate the modality discrepancy, which can be expressed as follows:

$$\mathbf{f}_{amp}^1 = Res_1(\mathbf{f}_{amp}), \quad \mathbf{f}_{amp}^2 = Res_2(\mathbf{f}_{amp}). \quad (6)$$

Then, these two amplitude components \mathbf{f}_{amp}^1 and \mathbf{f}_{amp}^2 are combined with the phase components \mathbf{f}_{pha} using IFFT to obtain two different spatial domain features, respectively. Finally, two parameter-shared batch normalization (BN) layers are applied to make the ANM module easier to optimize. Nevertheless, on the one hand, directly applying the IN layers to amplitude components \mathbf{f}_{amp}^1 and \mathbf{f}_{amp}^2 may damage some discriminative identity information, thereby adversely affecting the performance. On the other hand, such two convolutional branches cannot effectively mine the cross-modality nuances in the amplitude components.

To address the above issues, we propose a center-guided nuances mining loss \mathcal{L}_{cnm} to preserve discriminative identity information while discovering diverse cross-modality nuances. As shown in Fig. 4, taking the class centers \mathbf{c}_{v1} of feature \mathbf{f}_{v1} from one VIS branch as an example, the center-guided nuances mining loss can be formulated as follows:

$$\mathcal{L}_{cnm}(\mathbf{c}_{v1}) = \sum_{\substack{j,k=1, \\ y_j \neq y_k}}^P [2 \times D(\mathbf{c}_{v1}^j, \mathbf{c}_{i1}^j) - D(\mathbf{c}_{v1}^j, \mathbf{c}_{v2}^j) - D(\mathbf{c}_{v1}^j, \mathbf{c}_{i1}^k) + m]_+. \quad (7)$$

where $D(\cdot, \cdot)$ represents the Euclidean distance between two features. \mathbf{c}_{v1} and \mathbf{c}_{i1} are the class centers of the VIS and IR features from the same branch in a minibatch, respectively. \mathbf{c}_{v2} is the class centers of the VIS features from the other branch. j and k represent different classes in a minibatch. m is a margin hyperparameter to balance the three terms.

In Eq. (7), $\mathcal{L}_{cnm}(\mathbf{c}_{v1})$ can achieve diverse amplitude nuances mining by forcing the distances $D(\mathbf{c}_{v1}^j, \mathbf{c}_{v2}^j)$ between the same class centers \mathbf{c}_{v1}^j and \mathbf{c}_{v2}^j in the two branches from the VIS modality to be larger than the distances $D(\mathbf{c}_{v1}^j, \mathbf{c}_{i1}^j)$

between the class centers \mathbf{c}_{v1}^j and \mathbf{c}_{i1}^j of the VIS and IR modalities. Additionally, $\mathcal{L}_{cnm}(\mathbf{c}_{v1})$ can effectively alleviate the modality discrepancy between the VIS and IR features by forcing the distances $D(\mathbf{c}_{v1}^j, \mathbf{c}_{i1}^j)$ between the class centers \mathbf{c}_{v1}^j and \mathbf{c}_{i1}^j from the same class but different modalities in the two branches to be smaller than the distances $D(\mathbf{c}_{v1}^j, \mathbf{c}_{v1}^k)$ between the feature centers \mathbf{c}_{v1}^j and \mathbf{c}_{v1}^k from different classes in the same modality.

Similarly, for the class centers \mathbf{c}_{v2} , \mathbf{c}_{i1} and \mathbf{c}_{i2} of different branches, we can get its loss: $\mathcal{L}_{cnm}(\mathbf{c}_{v2})$, $\mathcal{L}_{cnm}(\mathbf{c}_{i1})$ and $\mathcal{L}_{cnm}(\mathbf{c}_{i2})$. Therefore, the final center-guided nuances mining loss \mathcal{L}_{cnm} can be formulated as follows:

$$\mathcal{L}_{cnm} = [\mathcal{L}_{cnm}(\mathbf{c}_{v1}) + \mathcal{L}_{cnm}(\mathbf{c}_{v2}) + \mathcal{L}_{cnm}(\mathbf{c}_{i1}) + \mathcal{L}_{cnm}(\mathbf{c}_{i2})]/4. \quad (8)$$

3.5. Multi-Loss Optimization

Besides the center-guided nuances mining loss \mathcal{L}_{cnm} , the cross-entropy loss \mathcal{L}_{id} and the triplet loss [14] \mathcal{L}_{tri} are also used to jointly optimize the proposed FDNM. Following [54, 62], we adopt the cross-entropy loss \mathcal{L}_{id} and the triplet loss \mathcal{L}_{tri} as our baseline loss for learning discriminative features. Therefore, the overall loss \mathcal{L}_{fdnm} for the proposed FDNM can be formulated as follows:

$$\mathcal{L}_{fdnm} = \mathcal{L}_{id} + \lambda_1 \mathcal{L}_{tri} + \lambda_2 \mathcal{L}_{cnm}, \quad (9)$$

where λ_1 and λ_2 are two hyperparameters to balance the relative importance of the loss terms \mathcal{L}_{tri} and \mathcal{L}_{cnm} .

4. Experiments

4.1. Datasets and Evaluation Metrics

The proposed FDNM method is evaluated on three challenging VIREID datasets, including SYSU-MM01 [41], RegDB [28] and LLCM [59]. The SYSU-MM01 dataset [41] includes 34,167 images of 491 identities. The training set contains 22,258 VIS images and 11,909 IR images of 395 identities, and the query set contains 3,803 IR images of 96 identities. Following [49], the gallery set includes the all-search mode and the indoor-search mode. The RegDB dataset [28] contains 8,240 images of 412 identities captured by a pair of overlapping VIS and IR cameras. Following [49], both VIS to IR and IR to VIS modes are used to evaluate the competing methods with a random half-half split of the training and testing set. The LLCM dataset [59] is a low-light cross-modality dataset, which contains 46,767 images of 1,064 identities. The training set includes 30,921 images of 713 identities, and the testing set includes 13,909 images of 351 identities. Both the VIS to IR and IR to VIS modes are used to evaluate the proposed FDNM method.

Following [54, 59], the standard cumulative matching characteristics (CMC) and the mean average precision (mAP) are used as the evaluation metrics.

Table 1. Comparisons with several state-of-the-art methods on the SYSU-MM01 (single-shot setting) and RegDB datasets. R-1, R-10, R-20 denotes the Rank-1, Rank-10, Rank-20 accuracy, respectively. The best and the second results are red and blue marked, respectively.

Methods	SYSU-MM01								RegDB							
	All Search				Indoor Search				VIS to IR				IR to VIS			
	R-1	R-10	R-20	mAP	R-1	R-10	R-20	mAP	R-1	R-10	R-20	mAP	R-1	R-10	R-20	mAP
D ² RL [38]	28.9	70.6	82.4	29.2	-	-	-	-	43.4	66.1	76.3	44.1	-	-	-	-
Hi-CMD [4]	34.9	77.6	-	35.9	-	-	-	-	70.9	86.4	-	66.0	-	-	-	-
AlignGAN [36]	42.4	85.0	93.7	40.7	45.9	87.6	94.4	54.3	57.9	-	-	53.6	56.3	-	-	53.4
cm-SSFT [25]	47.7	-	-	54.1	-	-	-	-	65.4	-	-	65.6	63.8	-	-	64.2
DDAG [52]	54.8	90.4	95.8	53.0	61.0	94.1	98.4	68.0	69.3	86.2	91.5	63.5	68.1	85.2	90.3	61.8
LbA [29]	55.4	-	-	54.1	58.5	-	-	66.3	74.2	-	-	67.6	67.5	-	-	72.4
NFS [2]	56.9	91.3	96.5	55.5	62.8	96.5	99.1	69.8	80.5	91.6	95.1	72.1	78.0	90.5	93.6	69.8
CoAL [39]	57.2	92.3	97.6	57.2	63.9	95.4	98.8	70.8	74.1	90.2	94.5	70.0	-	-	-	-
CM-NAS [9]	60.8	92.1	96.8	58.9	68.0	94.8	97.9	52.4	82.8	95.1	97.7	79.3	81.7	94.1	96.9	77.6
MCLNet [11]	65.4	93.3	97.1	62.0	72.6	97.0	99.2	76.6	80.3	92.7	96.0	73.1	75.9	90.9	94.6	69.5
FMCNet [58]	66.3	-	-	62.5	68.2	-	-	74.1	89.1	-	-	84.4	88.4	-	-	83.9
SMCL [40]	67.4	92.9	96.8	61.8	68.8	96.6	98.8	75.6	83.9	-	-	79.8	83.1	-	-	78.6
PMT [24]	67.5	95.4	98.6	65.0	71.7	96.7	99.3	76.5	84.8	-	-	76.6	84.2	-	-	75.1
DART [47]	68.7	96.4	99.0	66.3	72.5	97.8	99.5	78.2	83.6	-	-	75.7	82.0	-	-	73.8
MRCN [62]	68.9	95.2	98.4	65.5	76.0	98.3	99.7	79.8	91.4	98.0	99.0	84.6	88.3	96.7	98.5	81.9
CAJ [53]	69.9	95.7	98.5	66.9	76.3	97.9	99.5	80.4	85.0	95.5	97.5	79.1	84.8	95.3	97.5	77.8
MPANet [43]	70.6	96.2	98.8	68.2	76.7	98.2	99.6	81.0	82.8	-	-	80.7	83.7	-	-	80.9
MMN [60]	70.6	96.2	99.0	66.9	76.2	97.2	99.3	79.6	91.6	97.7	98.9	84.1	87.5	96.0	98.1	80.5
DCLNet [32]	70.8	-	-	65.3	73.5	-	-	76.8	81.2	-	-	74.3	78.0	-	-	70.6
MAUM [23]	71.7	-	-	68.8	77.0	-	-	81.9	87.9	-	-	85.1	87.0	-	-	84.3
DEEN [59]	74.7	97.6	99.2	71.8	80.3	99.0	99.8	83.3	91.1	97.8	98.9	85.1	89.5	96.8	98.4	83.4
MUN [57]	76.2	97.8	-	73.8	79.4	98.1	-	82.1	95.2	98.9	-	87.2	91.9	98.0	-	85.0
MSCLNet [61]	77.0	97.6	99.2	71.6	78.5	99.3	99.9	81.2	84.2	-	-	81.0	83.9	-	-	78.3
SGIEL [8]	77.1	97.0	99.1	72.3	82.1	97.4	98.9	83.0	92.2	-	-	86.6	91.1	-	-	85.2
FDNM (Ours)	77.8	97.8	99.6	75.1	87.3	99.4	100.0	89.1	95.5	99.0	99.6	90.0	94.0	98.5	99.3	88.7

4.2. Implementation Details

The proposed FDNM employs the two-stream ResNet50 network [12, 52] as the backbone network, which is initialized with pre-trained weights on ImageNet [5]. Following [33, 60, 62], all input images are resized to $3 \times 384 \times 192$, and the commonly used random grayscale, random horizontal flip and random erasing [63] are adopted for data augmentation techniques. During the training phase, 4 VIS images and 4 IR images of 6 identities are randomly sampled to build a mini-batch. The SGD optimizer is adopted and the momentum is set to 0.9. The initial learning rate is set to 1×10^{-2} and is linearly increased to 1×10^{-1} with 10 epochs. Then, the learning rate is respectively decayed to 1×10^{-2} , 1×10^{-3} and 1×10^{-4} after the 20th, 80th and 120th epochs, until a total of 150 epochs. For the hyperparameter λ_1 in Eq. (9), we experimentally set it to 1.0.

4.3. Comparison with State-of-the-Art Methods

To verify the superiority of the proposed FDNM, we compare it with several state-of-the-art methods. The quantitative results on the SYSU-MM01 and RegDB datasets are shown in Tab. 1, and the results on the LLCM dataset are shown in Tab. 2.

SYSU-MM01: From Tab. 1, we can observe that the

proposed FDNM achieves the best performance among all the competing methods. Specifically, for the all-search mode, FDNM achieves 77.8% in Rank-1 accuracy and 75.1% in mAP, surpassing the SGIEL [8] method by 0.7% in Rank-1 accuracy and the MUN [57] method by 1.3% in mAP, respectively. For the indoor-search mode, FDNM achieves 87.3% in Rank-1 accuracy and 89.1% in mAP, which outperforms the SGIEL [8] method by 5.2% in Rank-1 accuracy and the DEEN [59] method by 5.8% in mAP, respectively. The results show that the proposed FDNM is not only suitable for outdoor scenes, but also applicable for indoor scenes, exhibiting good generalization ability.

RegDB: From Tab. 1, we can observe that the proposed FDNM achieves the best performance against the state-of-the-art methods. Specifically, for the VIS to IR mode, FDNM achieves 95.5% in Rank-1 accuracy and 90.0% in mAP, which outperforms the second-best method (MUN [57]) by 2.8% in mAP. For the IR to VIS mode, the proposed FDNM obtains 94.0% in Rank-1 accuracy and 88.7% in mAP, which outperforms the MUN [57] method by 2.1% in Rank-1 accuracy and the SGIEL [8] method by 3.5% in mAP, respectively. The results validate the effectiveness of our method. Moreover, the results also demonstrate that the proposed FDNM can effectively alleviate the modality dis-

Table 2. Comparisons between the proposed FDNM and several state-of-the-art methods on the LLCM dataset.

Methods	IR to VIS				VIS to IR			
	R-1	R-10	R-20	mAP	R-1	R-10	R-20	mAP
DDAG [52]	42.4	72.7	80.6	49.0	51.4	81.5	88.3	38.8
LbA [29]	42.8	77.4	86.1	51.0	54.8	85.1	91.6	40.8
AGW [54]	49.1	79.1	85.9	55.8	63.7	88.7	92.8	47.2
CAJ [53]	49.9	78.9	85.8	56.4	63.7	88.0	92.4	47.7
MMN [60]	50.1	79.8	87.3	56.7	64.0	88.7	93.1	48.5
MRCN [62]	51.3	80.1	87.2	57.7	65.3	88.1	93.1	49.5
DART [47]	53.0	80.8	87.1	59.3	65.3	89.4	93.3	51.1
DEEN [59]	55.5	83.9	90.0	62.1	69.2	91.0	95.1	55.5
FDNM (Ours)	56.6	84.1	90.4	62.7	70.2	91.1	94.8	55.8

Table 3. Ablation studies for different components of the proposed FDNM on the SYSU-MM01 dataset.

Settings		All Search		Indoor Search				
Base.	Local	AGP	ANM	\mathcal{L}_{cnm}	R-1	mAP	R-1	mAP
✓					68.7	66.0	76.1	80.2
	✓				69.5	66.8	77.3	81.7
✓	✓				71.9	68.3	81.7	83.7
✓	✓	✓			74.6	71.7	84.2	87.1
✓	✓		✓		73.2	70.8	82.7	85.5
✓	✓		✓	✓	76.0	73.6	86.6	88.3
✓	✓	✓	✓	✓	77.8	75.1	87.3	89.1

crepancy between the VIS and IR images.

LLCM: From Tab. 2, we can observe that the proposed FDNM achieves competitive performance on the LLCM dataset. Specifically, for the IR to VIS mode, FDNM achieves 56.6% in Rank-1 accuracy and 62.7% in mAP, respectively. For the VIS to IR mode, FDNM obtains 70.2% in Rank-1 accuracy and 55.8% in mAP, respectively. Although DEEN [59] achieves an impressive performance through multi-branch networks and complex attention modules, it requires significant computational resources and training time. Compared with DEEN, the proposed FDNM is more effective and efficient for the VIREID task.

4.4. Ablation Studies

Ablation studies for the effectiveness of different components. To demonstrate the contribution of each component in FDNM, we conduct some ablation studies by evaluating different components on the SYSU-MM01 dataset. As we can see in Tab. 3, the “Base.” and “Local” represent the two-stream ResNet50 network [12, 52] with only global features or local features. The experiments show that: (1) the proposed AGP module can enhance the performance of the baseline by 2.7% in Rank-1 accuracy and 3.4% in mAP, which indicates the proposed AGP module can effectively alleviate the VIS-IR modality discrepancy by utilizing the key information in amplitude component to guide the phase component for learning discriminative feature representations. (2) The proposed ANM module slightly improves the performance of the baseline, but the results are not satisfactory. This is because directly applying the IN lay-

Table 4. Ablation studies with which block of ResNet-50 to integrate the proposed AGP module on the SYSU-MM01 dataset.

Settings	All Search		Indoor Search	
	R-1	mAP	R-1	mAP
baseline	71.9	68.3	81.7	83.7
AGP after block-0	72.3	69.1	82.1	84.5
AGP after block-1	74.1	71.3	83.8	86.4
AGP after block-2	73.1	70.9	82.9	86.0
AGP after block-3	71.1	68.5	80.2	82.5
AGP after block-4	70.8	67.2	79.5	81.7

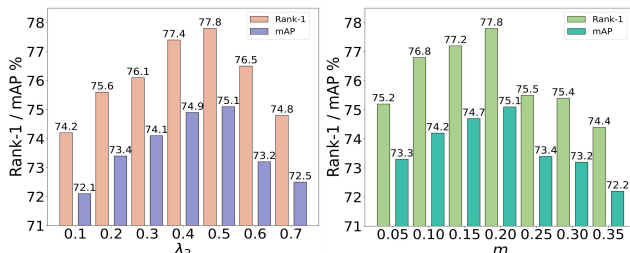


Figure 5. Comparisons of different λ_2 and m values on the SYSU-MM01 dataset.

ers to feature maps may corrupt some identity information and prevent the learning of discriminative feature representations. By contrast, the proposed center-guided nuances mining loss \mathcal{L}_{cnm} can greatly improve the performance of the ANM module. This shows that the \mathcal{L}_{cnm} loss can effectively mine the cross-modality nuances of the amplitude features while reducing the modality differences between the VIS and IR images. (3) By integrating the AGP module, the ANM module and the \mathcal{L}_{cnm} loss into an end-to-end frequency domain learning framework, the proposed FDNM effectively alleviates the modality discrepancy, resulting in a desirable performance.

Ablation studies with which block to integrate the AGP module. The proposed AGP module is a plug-and-play module and it can be integrated into any blocks of the backbone network. In our experiments, we utilize the two-stream ResNet-50 as the backbone, which includes 5 residual blocks: block-0 to block-4. To investigate the influence of integrating the proposed AGP module, we integrate it at different blocks. As shown in Tab. 4, when the AGP module is integrated after block-0 to block-2, the performance improves, suggesting that the key information in the amplitude component can effectively guide the phase component to learn discriminative feature representations. However, when the AGP module is integrated after block-3 and block-4, the performance drops rapidly. This is because integrating the AGP module after block-3 and block-4 may damage some discriminative phase information. Based on the above results, to balance the performance and efficiency, we integrate the proposed AGP module after the block-1 and block-2 of the backbone model.

The influence of the hyperparameters λ_2 and m . The proposed center-guided nuances mining loss \mathcal{L}_{cnm} utilizes

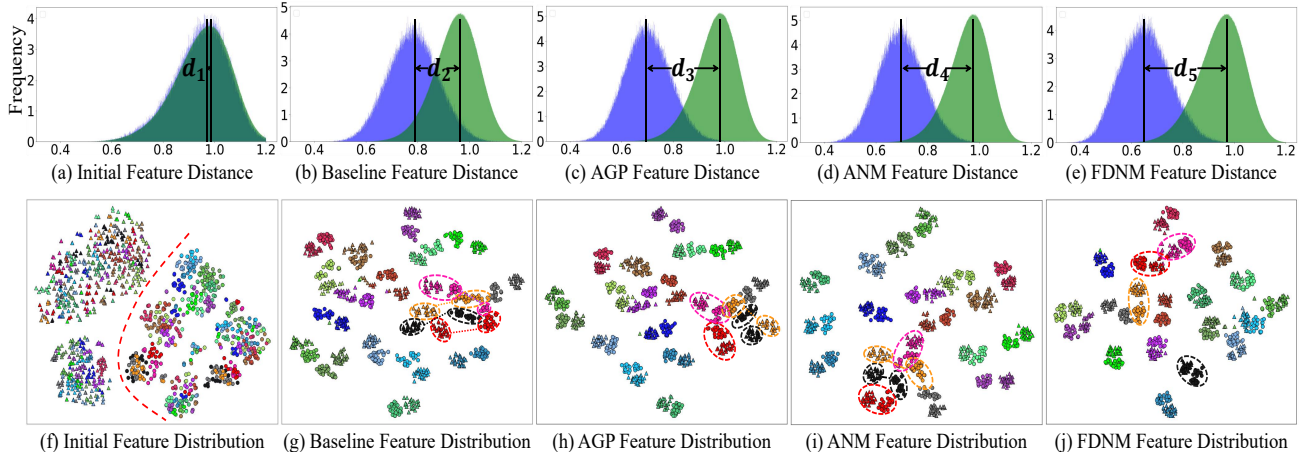


Figure 6. (a-e) The distribution of the cosine distance between VIS-IR intra-class features and inter-class features, which are indicated by blue and green colors, respectively. (f-j) The t-SNE [18] distribution of the VIS-IR features. Different colors represent different identities. The “circle” and “triangle” markers represent the VIS and IR features, respectively.

Table 5. Evaluation of the proposed FDNM on two visible-infrared face recognition datasets. The results of Rank-1 accuracy and false acceptance rate (F:%) are reported.

Methods	Oulu			BUAA		
	R-1	F:1%	F:0.1%	R-1	F:1%	F:0.1%
IDR [13]	94.3	73.4	46.2	94.3	93.4	84.7
ADFL [45]	95.5	83.0	60.7	95.2	95.3	88.0
PACH [6]	100	97.9	88.2	98.6	98.0	93.5
CAJ [53]	100	97.9	87.0	98.0	97.7	93.9
TOPLight [56]	100	98.9	91.7	98.3	98.0	94.6
LightCNN-29 [44]	100	97.9	87.0	98.0	97.7	93.7
FDNM (Ours)	100	99.1	92.2	99.8	98.9	95.5

two hyperparameters λ_2 and m with a triplet-like strategy to mine diverse nuances in the amplitude component. To evaluate the influence of λ_2 and m , we conduct quantitative comparisons and present the results in Fig. 5. As can be seen, with the increase of λ_2 and m values, the performance of FDNM gradually improves. However, when the values of λ_2 and m are more than a certain threshold, the performance of FDNM may collapse. Therefore, the values of λ_2 and m are set to 0.5 and 0.2, respectively.

4.5. Visualization Analysis

Intra-class and inter-class distances. To evaluate the effectiveness of the proposed method, we analyze the frequency distribution of the intra-class and inter-class distances between the VIS and IR features on SYSU-MM01. As shown in Fig. 6 (a-e). Compared the initial feature distances (Fig. 6 (a)) and baseline feature distances (Fig. 6 (b)) with the feature distances obtained by the proposed method Fig. 6 (c-e), the means (i.e., the vertical lines) of intra-class and inter-class distances are pushed away by using the proposed AGP module, ANM module and FDNM ($d_5 > d_3 > d_2 > d_1 \approx 0$, and $d_5 > d_4 > d_2 > d_1 \approx 0$). This result indicates that the proposed method can effectively al-

leviate the modality discrepancy between the VIS and IR images, thereby achieving better performance.

Feature distribution. For further validating the effectiveness of the proposed FDNM, we visualize the feature distribution utilizing t-SNE [18] on the SYSU-MM01 dataset. As shown in Fig. 6 (f-j), a total of 24 persons are randomly selected from the testing set of the SYSU-MM01 dataset. Compared with the initial feature distribution in Fig. 6 (f) and the baseline’s feature distribution in Fig. 6 (g), the feature distribution of the proposed AGP module, ANM module and FDNM can enlarge the distances between the features of different identities, and shorten the distances between the features from the same identities, which effectively reduce the VIS-IR modality discrepancies.

4.6. Visible-Infrared Face Recognition

To investigate the generalizability of the proposed FDNM, we evaluate it on two VIS-IR face recognition datasets (i.e., Oulu-CASIA NIR-VIS [1] and BUAA-VisNir [15]). Similar to [53, 56], we also adopt the LightCNN-29 [6, 44] as the backbone network for the VIS-IR face recognition task. The training details are exactly the same as [53, 56]. The results are shown in Tab. 5. As can be seen, the proposed FDNM can also enhance the performance of the VIS-IR face recognition task, which further indicates the effectiveness and generalization of the proposed FDNM.

5. Conclusion

In this paper, we aim to mine cross-modality frequency nuances for the VIREID task and propose a novel frequency domain nuances mining (FDNM) method. The proposed FDNM includes an amplitude guided phase module and an amplitude nuances mining module. These two modules are mutually beneficial to jointly reduce the VIS-IR modality

discrepancy. Besides, we propose a center-guided nuances mining loss to encourage the ANM module to preserve discriminative identity information while discovering diverse cross-modality nuances. Extensive experiments on three challenging VIREID datasets demonstrate the superior performance of the proposed FDNM method. Besides, we also validate the effectiveness and generalization of our method on the VIS-IR face recognition task.

References

- [1] Jie Chen, Dong Yi, Jimei Yang, Guoying Zhao, Stan Z. Li, and Matti Pietikainen. Learning mappings for face synthesis from near infrared to visual light images. In *CVPR*, pages 156–163, 2009. 8
- [2] Yehansen Chen, Lin Wan, Zhihang Li, Qianyan Jing, and Zongyuan Sun. Neural feature search for rgb-infrared person re-identification. In *CVPR*, pages 587–597, 2021. 1, 6
- [3] De Cheng, Xiaolong Wang, Nannan Wang, Zhen Wang, Xiaoyu Wang, and Xinbo Gao. Cross-modality person re-identification with memory-based contrastive embedding. In *AAAI*, pages 425–432, 2023. 1
- [4] Seokeon Choi, Sumin Lee, Youngeun Kim, Taekyung Kim, and Changick Kim. Hi-cmd: Hierarchical cross-modality disentanglement for visible-infrared person re-identification. In *CVPR*, pages 10257–10266, 2020. 2, 6
- [5] Jia Deng, Wei Dong, Richard Socher, Li-Jia Li, Kai Li, and Li Fei-Fei. Imagenet: A large-scale hierarchical image database. In *CVPR*, pages 248–255, 2009. 6
- [6] Boyan Duan, Chaoyou Fu, Yi Li, Xingguang Song, and Ran He. Cross-spectral face hallucination via disentangling independent factors. In *CVPR*, 2020. 8
- [7] Xingye Fang, Yang Yang, and Ying Fu. Visible-infrared person re-identification via semantic alignment and affinity inference. In *ICCV*, pages 11270–11279, 2023. 3
- [8] Jiawei Feng, Ancong Wu, and Wei-Shi Zheng. Shape-erased feature learning for visible-infrared person re-identification. In *CVPR*, pages 22752–22761, 2023. 2, 6
- [9] Chaoyou Fu, Yibo Hu, Xiang Wu, Hailin Shi, Tao Mei, and Ran He. Cm-nas: Cross-modality neural architecture search for visible-infrared person re-identification. In *ICCV*, pages 11823–11832, 2021. 6
- [10] Yajun Gao, Tengfei Liang, Yi Jin, Xiaoyan Gu, Wu Liu, Yidong Li, and Congyan Lang. Mso: Multi-feature space joint optimization network for rgb-infrared person re-identification. In *ACM MM*, pages 5257–5265, 2021. 2
- [11] Xin Hao, Sanyuan Zhao, Mang Ye, and Jianbing Shen. Cross-modality person re-identification via modality confusion and center aggregation. In *CVPR*, pages 16403–16412, 2021. 1, 6
- [12] Kaiming He, Xiangyu Zhang, Shaoqing Ren, and Jian Sun. Deep residual learning for image recognition. In *CVPR*, pages 770–778, 2016. 6, 7
- [13] Ran He, Xiang Wu, Zhenan Sun, and Tieniu Tan. Learning invariant deep representation for nir-vis face recognition. In *AAAI*, page 2000–2006, 2017. 8
- [14] Alexander Hermans, Lucas Beyer, and Bastian Leibe. In defense of the triplet loss for person re-identification. *ArXiv*, 2017. 5
- [15] D Huang, J Sun, and Y Wang. The buaa-visnir face database instructions. *School Comput. Sci. Eng., Beihang Univ., Beijing, China, Tech. Rep. IRIP-TR-12-FR-001*, 3(3):8, 2012. 8
- [16] Jie Huang, Yajing Liu, Feng Zhao, Keyu Yan, Jinghao Zhang, Yukun Huang, Man Zhou, and Zhiwei Xiong. Deep fourier-based exposure correction network with spatial-frequency interaction. In *ECCV*, pages 163–180, 2022. 1, 3
- [17] Minsu Kim, Seungryong Kim, Jungin Park, Seongheon Park, and Kwanghoon Sohn. Partmix: Regularization strategy to learn part discovery for visible-infrared person re-identification. In *CVPR*, pages 18621–18632, 2023. 2
- [18] Van Der Maaten Laurens and Geoffrey Hinton. Visualizing data using t-sne. In *JMLR*, pages 2579–2605, 2008. 2, 8
- [19] Sangrok Lee, Jongseong Bae, and Ha Young Kim. Decompose, adjust, compose: Effective normalization by playing with frequency for domain generalization. In *CVPR*, pages 11776–11785, 2023. 1
- [20] Diangang Li, Xing Wei, Xiaopeng Hong, and Yihong Gong. Infrared-visible cross-modal person re-identification with an x modality. In *AAAI*, pages 4610–4617, 2020. 2
- [21] Yulin Li, Tianzhu Zhang, and Yongdong Zhang. Frequency domain modality-invariant feature learning for visible-infrared person re-identification. *ArXiv*, 2024. 3
- [22] Chengxu Liu, Xuan Wang, Shuai Li, Yuzhi Wang, and Xueming Qian. Fsi: Frequency and spatial interactive learning for image restoration in under-display cameras. In *ICCV*, pages 12537–12546, 2023. 3
- [23] Jialun Liu, Yifan Sun, Feng Zhu, Hongbin Pei, Yi Yang, and Wenhui Li. Learning memory-augmented unidirectional metrics for cross-modality person re-identification. In *CVPR*, pages 19366–19375, 2022. 6
- [24] Hu Lu, Xuezhong Zou, and Pingping Zhang. Learning progressive modality-shared transformers for effective visible-infrared person re-identification. In *AAAI*, pages 1835–1843, 2023. 1, 6
- [25] Yan Lu, Yue Wu, Bin Liu, Tianzhu Zhang, Baopu Li, Qi Chu, and Nenghai Yu. Cross-modality person re-identification with shared-specific feature transfer. In *CVPR*, pages 13379–13389, 2020. 6
- [26] Hao Luo, Youzhi Gu, Xingyu Liao, Shenqi Lai, and Wei Jiang. Bag of tricks and a strong baseline for deep person re-identification. In *CVPR Workshops*, pages 1487–1495, 2019. 4
- [27] Ziling Miao, Hong Liu, Wei Shi, Wanlu Xu, and Hanrong Ye. Modality-aware style adaptation for rgb-infrared person re-identification. In *IJCAI*, pages 19–27, 2021. 2
- [28] Dat Tien Nguyen, Hyung Gil Hong, Ki Wan Kim, and Kang Ryoung Park. Person recognition system based on a combination of body images from visible light and thermal cameras. *Sensors*, 17(3):605, 2017. 5, 1
- [29] Hyunjong Park, Sanghoon Lee, Junghyup Lee, and Bumsub Ham. Learning by aligning: Visible-infrared person re-identification using cross-modal correspondences. In *ICCV*, pages 12046–12055, 2021. 6, 7

- [30] Nan Pu, Wei Chen, Yu Liu, Erwin M Bakker, and Michael S Lew. Dual gaussian-based variational subspace disentanglement for visible-infrared person re-identification. In *ACM MM*, pages 2149–2158, 2020. [2](#)
- [31] Jiangming Shi, Yachao Zhang, Xiangbo Yin, Yuan Xie, Zhizhong Zhang, Jianping Fan, Zhongchao Shi, and Yanyun Qu. Dual pseudo-labels interactive self-training for semi-supervised visible-infrared person re-identification. In *ICCV*, pages 11218–11228, 2023. [1](#)
- [32] Hanzhe Sun, Jun Liu, Zhizhong Zhang, Chengjie Wang, Yanyun Qu, Yuan Xie, and Lizhuang Ma. Not all pixels are matched: Dense contrastive learning for cross-modality person re-identification. In *ACM MM*, page 5333–5341, 2022. [6](#)
- [33] Lei Tan, Yukang Zhang, Shengmei Shen, Yan Wang, Pingyang Dai, Xianming Lin, Yongjian Wu, and Rongrong Ji. Exploring invariant representation for visible-infrared person re-identification. *ArXiv*, 2023. [6](#)
- [34] Dmitry Ulyanov, Andrea Vedaldi, and Victor Lempitsky. Instance normalization: The missing ingredient for fast stylization. *ArXiv*, 2016. [5](#)
- [35] Chenyang Wang, Junjun Jiang, Zhiwei Zhong, and Xianming Liu. Spatial-frequency mutual learning for face super-resolution. In *CVPR*, pages 22356–22366, 2023. [3](#)
- [36] Guan-An Wang, Tianzhu Zhang, Jian Cheng, Si Liu, Yang Yang, and Zengguang Hou. Rgb-infrared cross-modality person re-identification via joint pixel and feature alignment. In *ICCV*, pages 3623–3632, 2019. [2, 6](#)
- [37] Guan-An Wang, Tianzhu Zhang, Jian Cheng, Jianlong Chang, Xu Liang, Zengguang Hou, et al. Cross-modality paired-images generation for rgb-infrared person re-identification. In *AAAI*, pages 12144–12151, 2020.
- [38] Zhixiang Wang, Zheng Wang, Yinqiang Zheng, Yung-Yu Chuang, and Shin’ichi Satoh. Learning to reduce dual-level discrepancy for infrared-visible person re-identification. In *CVPR*, pages 618–626, 2019. [2, 6](#)
- [39] Xing Wei, Diangang Li, Xiaopeng Hong, Wei Ke, and Yihong Gong. Co-attentive lifting for infrared-visible person re-identification. In *ACM MM*, pages 1028–1037, 2020. [6](#)
- [40] Ziyu Wei, Xi Yang, Nannan Wang, and Xinbo Gao. Syncretic modality collaborative learning for visible infrared person re-identification. In *ICCV*, pages 225–234, 2021. [2, 6](#)
- [41] Ancong Wu, Wei-Shi Zheng, Hong-Xing Yu, Shaogang Gong, and Jianhuang Lai. Rgb-infrared cross-modality person re-identification. In *ICCV*, pages 5380–5389, 2017. [5, 1](#)
- [42] Jianbing Wu, Hong Liu, Yuxin Su, Wei Shi, and Hao Tang. Learning concordant attention via target-aware alignment for visible-infrared person re-identification. In *ICCV*, pages 11122–11131, 2023. [2](#)
- [43] Qiong Wu, Pingyang Dai, Jie Chen, Chia-Wen Lin, Yongjian Wu, Feiyue Huang, Bineng Zhong, and Rongrong Ji. Discover cross-modality nuances for visible-infrared person re-identification. In *CVPR*, pages 4330–4339, 2021. [6](#)
- [44] Xiang Wu, Ran He, Zhenan Sun, and Tieniu Tan. A light cnn for deep face representation with noisy labels. *TIFS*, 13(11): 2884–2896, 2018. [8](#)
- [45] Xiang Wu, Lingxiao Song, Ran He, and Tieniu Tan. Coupled deep learning for heterogeneous face recognition. In *AAAI*, page 1679–1686, 2018. [8](#)
- [46] Bin Yang, Jun Chen, and Mang Ye. Towards grand unified representation learning for unsupervised visible-infrared person re-identification. In *ICCV*, pages 11069–11079, 2023. [2](#)
- [47] Mouxing Yang, Zhenyu Huang, Peng Hu, Taihao Li, Jiancheng Lv, and Xi Peng. Learning with twin noisy labels for visible-infrared person re-identification. In *CVPR*, pages 14308–14317, 2022. [6, 7](#)
- [48] Mingde Yao, Jie Huang, Xin Jin, Ruikang Xu, Shenglong Zhou, Man Zhou, and Zhiwei Xiong. Generalized lightness adaptation with channel selective normalization. In *ICCV*, pages 10668–10679, 2023. [3](#)
- [49] Mang Ye, Xiangyuan Lan, Jiawei Li, and Pong C Yuen. Hierarchical discriminative learning for visible thermal person re-identification. In *AAAI*, pages 7501–7508, 2018. [1, 5](#)
- [50] Mang Ye, Zheng Wang, Xiangyuan Lan, and Pong C Yuen. Visible thermal person re-identification via dual-constrained top-ranking. In *IJCAI*, pages 1092–1099, 2018. [1](#)
- [51] Mang Ye, Xiangyuan Lan, and Qingming Leng. Modality-aware collaborative learning for visible thermal person re-identification. In *ACM MM*, pages 347–355, 2019. [2](#)
- [52] Mang Ye, Jianbing Shen, David J Crandall, Ling Shao, and Jiebo Luo. Dynamic dual-attentive aggregation learning for visible-infrared person re-identification. In *ECCV*, pages 229–247, 2020. [6, 7](#)
- [53] Mang Ye, Weijian Ruan, Bo Du, and Mike Zheng Shou. Channel augmented joint learning for visible-infrared recognition. In *ICCV*, pages 13567–13576, 2021. [6, 7, 8](#)
- [54] Mang Ye, Jianbing Shen, Gaojie Lin, Tao Xiang, Ling Shao, and Steven CH Hoi. Deep learning for person re-identification: A survey and outlook. *TPAMI*, 44(6):2872–2893, 2021. [5, 7](#)
- [55] Hu Yu, Naishan Zheng, Man Zhou, Jie Huang, Zeyu Xiao, and Feng Zhao. Frequency and spatial dual guidance for image dehazing. In *ECCV*, pages 181–198, 2022. [1, 3, 4](#)
- [56] Hao Yu, Xu Cheng, and Wei Peng. Toplight: Lightweight neural networks with task-oriented pretraining for visible-infrared recognition. In *CVPR*, pages 3541–3550, 2023. [8](#)
- [57] Hao Yu, Xu Cheng, Wei Peng, Weihao Liu, and Guoying Zhao. Modality unifying network for visible-infrared person re-identification. In *ICCV*, pages 11185–11195, 2023. [6](#)
- [58] Qiang Zhang, Changzhou Lai, Jianan Liu, Nianchang Huang, and Jungong Han. Fmcnet: Feature-level modality compensation for visible-infrared person re-identification. In *CVPR*, pages 7349–7358, 2022. [6](#)
- [59] Yukang Zhang and Hanzi Wang. Diverse embedding expansion network and low-light cross-modality benchmark for visible-infrared person re-identification. In *CVPR*, pages 2153–2162, 2023. [2, 5, 6, 7, 1](#)
- [60] Yukang Zhang, Yan Yan, Yang Lu, and Hanzi Wang. Towards a unified middle modality learning for visible-infrared person re-identification. In *ACM MM*, pages 788–796, 2021. [2, 6, 7](#)
- [61] Yiyuan Zhang, Sanyuan Zhao, Yuhao Kang, and Jianbing Shen. Modality synergy complement learning with cascaded

- aggregation for visible-infrared person re-identification. In *ECCV*, pages 462–479, 2022. 6
- [62] Yukang Zhang, Yan Yan, Jie Li, and Hanzi Wang. Mrcn: A novel modality restitution and compensation network for visible-infrared person re-identification. In *AAAI*, 37(3): 3498–3506, 2023. 5, 6, 7
- [63] Zhun Zhong, Liang Zheng, Guoliang Kang, Shaozi Li, and Yi Yang. Random erasing data augmentation. In *AAAI*, pages 13001–13008, 2020. 6
- [64] Man Zhou, Jie Huang, Keyu Yan, Hu Yu, Xueyang Fu, Aiping Liu, Xian Wei, and Feng Zhao. Spatial-frequency domain information integration for pan-sharpening. In *ECCV*, pages 274–291, 2022. 3, 4

Frequency Domain Nuances Mining for Visible-Infrared Person Re-identification

Supplementary Material

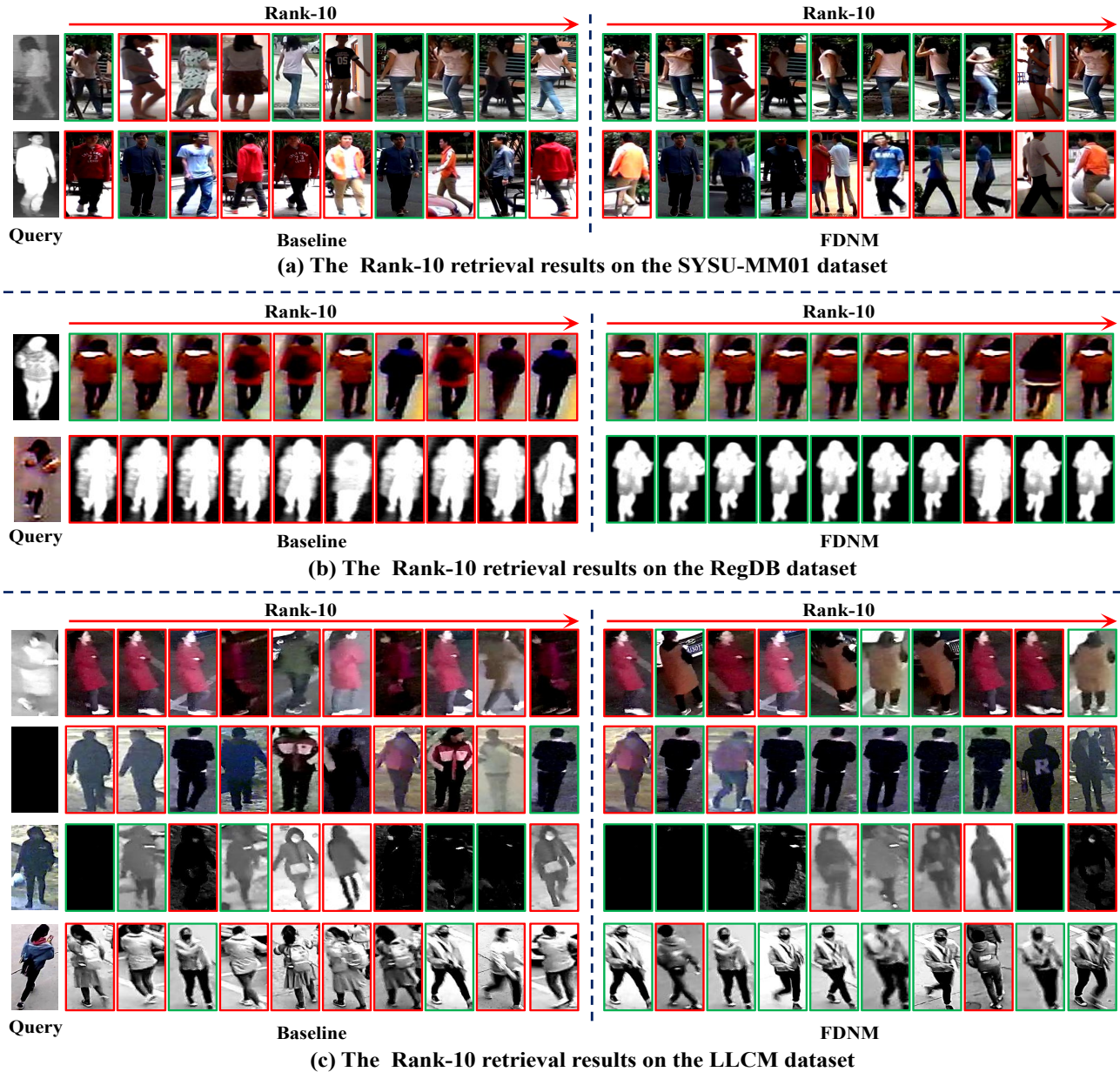


Figure 7. The Rank-10 retrieval results obtained by the baseline method and the proposed FDNM method on the SYSU-MM01 (under the multi-shot setting and the all-search mode), RegDB and LLCM datasets.

6. Retrieval results

To further evaluate the proposed FDNM, we compare the retrieval results obtained by our method with those obtained by the baseline method on several VIS-IR image pairs from

the SYSU-MM01 [41] (under the multi-shot setting and the all-search mode), RegDB [28] and LLCM datasets [59]. For the RegDB and LLCM datasets, both the VIS to IR and IR to VIS modes are evaluated. The results are shown in Fig. 7.

For each retrieval case, the query images shown in the first column are given images, and the gallery images shown in the following columns are retrieved images obtained by the baseline method and the proposed FDNM method. The retrieved images with the green bounding boxes belong to the same identities as the query images, while the images with the red bounding boxes are opposite to the query images. The experiments show that:

(1) In general, the proposed FDNM method can effectively improve the ranking results with more green bounding boxes ranked in the top positions on those three challenging VIREID datasets, which demonstrates that the proposed FDNM can effectively alleviate the modality discrepancy between the VIS and IR images and improve the performance of the VIREID task.

(2) The proposed FDNM is not only suitable for the VIS and NIR (near infrared) match tasks such as for the SYSU-MM01 and LLCM datasets, but also applicable for the VIS and TIR (thermal infrared) match tasks such as for the RegDB dataset, exhibiting good generalization ability.

(3) The ranking results obtained by the proposed FDNM method on the LLCM dataset with more green bounding boxes ranked in the top positions, which indicates that the proposed FDNM method also has good robustness and generalization to extremely low-light environments at night.